

RESEARCH ARTICLE

Stochastic Parameterization of Column Physics using Generative Adversarial Networks

Balasubramanya T. Nadiga^{1*}, Xiaoming Sun¹ and Cody Nash²

¹Los Alamos National Laboratory, Los Alamos, 87545, NM, USA

²Independent Researcher, Topol'čany, 95501, Slovakia

*Corresponding author. Email: balu@lanl.gov

Received: 28 January 2022

Keywords: column physics, stochastic parameterization, machine learning, generative adversarial network

Abstract

We demonstrate the use of a probabilistic machine learning technique to develop stochastic parameterizations of atmospheric column-physics. After suitable preprocessing of NASA's Modern-Era Retrospective analysis for Research and Applications, version 2 (MERRA2) data to minimize the effects of high-frequency, high-wavenumber component of MERRA2 estimate of vertical velocity, we use generative adversarial networks to learn the probability distribution of vertical profiles of diabatic sources conditioned on vertical profiles of temperature and humidity. This may be viewed as an improvement over previous similar but deterministic approaches that seek to alleviate both, shortcomings of human-designed physics parameterizations, and the computational demand of the “physics” step in climate models.

Impact Statement

Global climate models can now be used to produce realistic simulations of climate. However, large uncertainties remain: e.g., the estimated change in globally-averaged-surface-temperature to a doubling of atmospheric CO₂ varies between ~2 and ~6 degrees-Centigrade across leading models. Uncertainty in representing cumulus convection (think thunderstorm) is a major contributor to this spread: Scales at which they occur, 100m-10km, are too small to be resolved in global climate models, requiring their effects on larger scales to be approximated with simple models. Improving such approximations using new probabilistic machine learning techniques, initial steps towards which are successfully demonstrated in this work, will likely lead to improvements in the modeling of climate through improvements in the representation of cumulus convection in climate models.

1. Introduction and Problem Formulation

Over the past 70 years, there has been a concerted effort to develop first principles based models of Earth's climate. In this ongoing effort, current (state-of-the-art, SOTA) comprehensive climate models and Earth System Models (ESMs) have achieved a level of sophistication and realism that they are proving invaluable in improving our understanding of various processes underlying the climate system and its variability (Chen et al., 2021, pg. 82). Limited by computational resources, however, most comprehensive climate simulations are currently conducted with horizontal grid spacings of between 50 and 100 km in the atmosphere. However, many atmospheric processes occur at much smaller scales.

These include cumulus convection, boundary layer turbulence, cloud microphysics, and others. Even as resolutions continue to slowly increase, a number of these small-scale processes are not expected to be explicitly resolved in long-term simulations of climate for a long time. As such, the effects of such unresolved subgrid processes on the resolved scales have to be represented using parameterizations.

To wit, the evolution of temperature T and moisture (represented by specific humidity) q may be written as (e.g., see Yanai et al., 1973; Nitta, 1977)

$$\frac{\partial T}{\partial t} + u \frac{\partial T}{\partial x} + v \frac{\partial T}{\partial y} - \omega S_p = q_1, \quad (1)$$

$$\frac{\partial q}{\partial t} + u \frac{\partial q}{\partial x} + v \frac{\partial q}{\partial y} - \omega \frac{\partial q}{\partial p} = -q_2. \quad (2)$$

Here, (u, v) is the horizontal velocity field, ω is the vertical velocity in pressure coordinates, S_p is static stability given by $S_p = -\frac{T}{\theta} \frac{\partial \theta}{\partial p}$, where θ is potential temperature and other notation is standard. To simplify notation, in the above equations all variables on the left hand side (LHS) are understood to be variables at the resolved scale. With that convention, q_1 and q_2 are parameterizations that represent the effect of unresolved subgrid processes on the evolution of resolved scale temperature and moisture. (Additional mass and momentum conservation equations complete the system, e.g., by providing the evolution of (u, v, ω) .) For convenience, following (Yanai et al., 1973), we refer to q_1 as apparent heating and q_2 as apparent moisture sink.

In the above equations, terms on the LHS represent slow, large-scale dynamical evolution. Phenomenologically, when the large-scale dynamical evolution or forcing serves to set-up conditions that are convectively unstable, the system responds by locally and intermittently forming cumulus convective updrafts that serve to locally resolve or eliminate the instability. Indeed, the interaction between the large-scale dynamics and small-scale intermittent moist nonhydrostatic cumulus response continues over a range of subgrid scales, from minutes and hundreds of meters to hours and up to ten kilometers. Thus, from the point of view of the equations above, q_1 and q_2 represent the effect of unresolved cumulus and other subgrid processes on the evolution of the vertical profiles of environmental averages of the thermodynamic variables T and q ; q_1 is an apparent heating source and q_2 is an apparent moisture sink. In particular, q_1 comprises effects of radiative and latent heating and vertical turbulent heat flux, and q_2 effects of latent heating. The effects of horizontal turbulent transport are smaller in comparison and are therefore commonly neglected, as we do here.

In SOTA climate models, forward evolution of the atmospheric state over each timestep consists of a “dynamics” update (solving the mass and momentum equations and computing terms on the LHS of Eqs. 1 and 2) followed by a “physics” update. It is the “physics” update—effectively computing q_1 and q_2 —that implements the various schemes that capture the effect of unresolved dynamical and thermodynamic processes (e.g., turbulence transport including that of convective updrafts, various boundary layer processes, cloud microphysics, radiation. etc.) on the resolved scales. Physics parameterizations in SOTA climate models tends to be one of the most computationally intensive parts (e.g., see Bosler et al., 2019; Bradley et al., 2019). Furthermore, since traditional parameterizations are based on our limited understanding of the complex subgrid-scale processes, significant inaccuracies persist in the representation of microphysics, cumulus, boundary layer, and other processes (e.g., Sun and Barros, 2014). Indeed, as pointed out by Sherwood et al. (2014), uncertainty in cumulus parameterization is a major source of spread in climate sensitivity of ESMs that are used for climate projections for the 21st century.

The recent explosion of research in machine learning (ML) has naturally led to the examination of the use of ML in alleviating both, shortcomings of human-designed physics parameterizations, and the computational demand of the “physics” step in climate models. In this context, recent research has focussed on using short high resolution simulations of climate that resolve convective updrafts, commonly called cloud resolving models (CRM) as ground truth for developing a computational-cheaper, unified machine learned parameterization that replaces the traditional “physics” step. For example,

using this approach, Brenowitz and Bretherton (2018) (BB18) were able to improve the representation of temperature and humidity fields when compared with traditional physics parameterizations.

In this study, instead of using output from high-resolution CRMs, since CRMs can themselves deviate from reality in many aspects (e.g., Lean et al., 2008; Weisman et al., 2008; Herman and Schumacher, 2016; Zhang et al., 2016), we train a ML model using reanalysis fields from the Modern-Era Retrospective Analysis for Research and Applications version 2 (MERRA-2, Rienecker et al. (2011)). Further, two similar input profiles (of temperature and humidity) can evolve differently due to chaotic subgrid cumulus dynamics and result in different output profiles (of apparent heating and apparent moisture sink). As such, we estimate q_1 and q_2 using a probabilistic ML model. This choice is also consistent with the suggestion that a stochastic approach is likely more appropriate for parameterizations in terms of reducing the uncertainties stemming from the lack of scale separation between resolved and unresolved processes (e.g., see Nadiga and Livescu, 2007; Duan and Nadiga, 2007; Nadiga, 2008; Palmer, 2019).

2. The Tropical Eastern Pacific, Data and Preprocessing

The inter-tropical convergence zone (ITCZ) is one of the easily-recognized large-scale features of earth's atmospheric circulation. It appears as a zonally-elongated band of clouds that at times even encircles the globe. It comprises of thunderstorm systems with low level convergence, and intense convection and precipitation. The domain we choose—the region of Eastern Pacific, 15S-15N and 180-100.25W—includes both a segment of the more coherent northern branch of the ITCZ as a band across the northern part of the domain, and a segment of the more seasonal southern branch in the southwestern part of the domain. In the top-left panel of Fig. 1, which show the 2003 annual mean of column-averaged specific humidity, the ITCZ is contained in the broad and diffuse bands of high moisture seen in yellow. While not evident in the equivalently averaged temperature field (top-right), it is better identified in the q_1 and q_2 fields (bottom row; see later). To aid in geo-locating the domain considered and the ITCZ, the inset in the bottom-right panel shows the q_1 field for January 1st, 2003 on a map with the coastlines of the Americas.

Whereas the timescales of convective updrafts range from minutes to hours, the reanalyzed fields under NASA's Modern-Era Retrospective analysis for Research and Applications, version 2 (MERRA2) project are made available at a sampling interval of 3 hours. Nevertheless, the reanalyzed fields contain the averaged effects of convective updrafts and other subgrid processes. First, we use the T , q , and (u, v, ω) fields to estimate q_1 and q_2 using Eqs. 1 and 2. On so doing, we find that there are numerous instances wherein the diagnosed q_1 and q_2 fields are dominated by the vertical advection of temperature and specific humidity respectively, and which are themselves much larger than the horizontal advection terms and the temporal tendency terms. Furthermore, in such cases, the vertical distributions of q_1 and q_2 were found to be highly correlated to the vertical distributions of vertical advection of temperature and specific humidity respectively. We proceed to further investigate this aspect of the diagnosed diabatic sources in order to establish that they are not mere artifacts before proceeding with modeling them.

MERRA2 is a reanalysis product in the sense that it uses an atmospheric general circulation model (AGCM), the Goddard Earth Observing System version 5 (GEOS-5) and assimilates observations to produce interpolated and regularly-gridded data (Rienecker et al., 2011). While vertical motion is intimately linked to the stability of the atmosphere given stratification in the vertical, and is key to the formation of cumulus, vertical velocity is usually not directly measured. It is indeed the case that direct observations of vertical motion are not part of the data that are assimilated by the GOES-5 AGCM to produce MERRA2. As such, to examine whether the high frequency (temporal), high-wavenumber (spatial) component of the inferred vertical (pressure) velocity of MERRA2 (components in which the confidence tends to be lower than in the slower, larger-scale components) leads to the correlation mentioned above, we consider further spatiotemporal averaging of the MERRA2 fields from a native

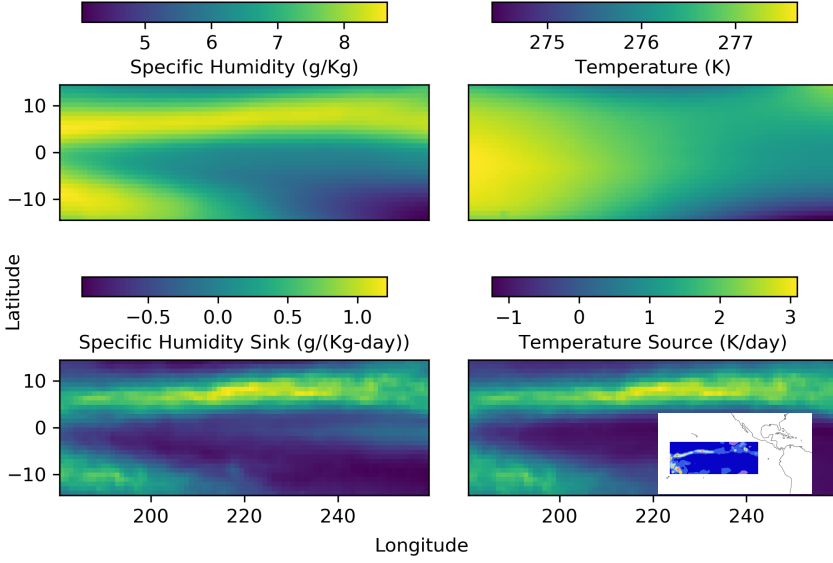


Figure 1. Preprocessing of MERRA2 data in the tropical Eastern Pacific. Top: Annual mean of column-averaged specific humidity (left) and temperature (right) in the Eastern Pacific. Bottom: Annual mean of apparent moisture sink (left) and apparent heating (right). To aid in geo-locating the domain considered and the ITCZ, the inset in the bottom-right panel shows the q_1 field for January 1st, 2003 on a map.

resolution of 0.5×0.625 degrees at 3 hours to a daily average at a coarsened resolution of 1×1 degree (e.g., [Sun and Barros, 2015](#)). The persistence of the correlations, however, suggests that the correlations are likely real.

All fields are considered on MERRA2’s native vertical grid (pressure levels) and we confine attention to the troposphere, defined here for convenience as pressure levels deeper than 190 mbar (hPa); there are 31 such levels. Figure 1 shows the annual and vertical average of specific humidity (top-left), temperature (top-right), diagnosed specific humidity sink (bottom-left), and temperature source (bottom-right). The ITCZ is seen to be better defined in the diagnosed (bottom) fields and its structure in q_1 and q_2 is also seen to be highly correlated.

3. Generative Adversarial Networks

The governing equations would be closed if we are able to express the three-dimensional fields q_1 and q_2 in terms of the resolved (3D) variables; given that they are not closed, we proceed to find such closures using machine-learning. However, given the physics of the problem described previously, the dominant variation of such relationships is captured by the column-wise variation of q_1 and q_2 in terms of the column-wise variation of T and q . Furthermore, as alluded to earlier, we should not expect unique functional relationships between the predictands and predictors. As such a probabilistic ML framework is called for. That is, instead of learning maps

$$[T(p), q(p)] \mapsto [q_1(p), q_2(p)],$$

we are led to want to learn the conditional probability

$$P([q_1(p), q_2(p)] | [T(p), q(p)]),$$

the probability of $[q_1(p), q_2(p)]$ occurring given the occurrence of conditions $[T(p), q(p)]$.

In this setting, a conditional generative model is required, since in essence, a generative model learns a representation of the *unknown probability distribution* of the data. Different classes of generative

models have been developed and they can range from generative adversarial networks (GANs) (Goodfellow et al., 2014) to variational autoencoders (Kingma and Welling, 2013) to continuous normalizing flows (Rezende and Mohamed, 2015) to diffusion maps (Coifman and Lafon, 2006) and others. However, we choose GANs since they have been investigated more extensively than the others. As a class of generative models, GANs are trained using an adversarial technique: while a discriminator continually learns to discriminate between the generator's synthetic output and true data, given a noise source, the generator progressively seeks to fool the discriminator by synthesizing yet more realistic samples. The (dual) learning progresses until quasi-equilibrium is reached (see Fig. 2a for an example of this in the current setup), wherein the discriminator's feedback to the generator does not permit further large improvements of the generator, but rather leads to stochastic variations that explore the local basin of attraction. In this state, the training of the generator may be considered as successful to the extent that the discriminator has a hard time, both, discriminating between true samples and fake samples created by the trained generator, and learning further to discriminate them.

Initially, the training of GANs was problematic in that they commonly suffered from instability and various modes of failure. One of the approaches developed in response to the problem of instability in the training of GANs was the Wasserstein GAN (WGAN) (Arjovsky and Bottou, 2017). The WGAN approach leverages the Wasserstein distance (Kantorovitch, 1958) on the space of probability distributions to produce a value function that has better theoretical properties, and requires the discriminator (called the critic in the WGAN setting) to lie in the space of 1-Lipschitz functions. While the WGAN approach made significant progress towards stable training of GANs and gained popularity, subsequent accumulating evidence revealed that the WGAN approach could sometimes generate only poor samples or, worse, even fail to converge. In further response to this aspect of WGANs, a variation of the WGAN was proposed in Gulrajani et al. (2017): while in the original WGAN, a weight-clipping approach was used to ensure that the critic lay in the space of 1-Lipschitz functions, the new approach used a gradient penalty term in the critic's loss function to satisfy the 1-Lipschitz requirement. As such this approach was called the Wasserstein GAN with gradient penalty (WGAN-GP).

3.1. Architecture and Loss Functions

In the conditional version of the WGAN-GP we use, besides the input and output layers, the generator and critic networks each consist of three fully connected feed-forward hidden layers (multi-layer perceptron architecture). The hidden layers have 512 neurons each with 10% dropout, and use rectified linear unit (ReLU) activation functions while the input and output layers are linear. The noise sample was concatenated to the condition vector for input to the generator. And, the condition vector was concatenated to the real or generated sample to form the input to the critic network.

The dataset consisted of 864,000 datapoints (30 latitude bins, 80 longitude bins, and 360 daily averages (1/4-12/29)) with 62 conditions representing temperature and humidity at 31 vertical pressure levels. The target variables were q_1 and q_2 at the same 31 vertical levels. To account for the typical dominant nature of the seasonal component of climate variability, the dataset was split into quarters, the first 70 days of each quarter were used for training and the subsequent 20 days of each quarter constituted the test set. Training data was scaled to a mean of zero and unit standard deviation (standardized), and the same, learned, transformation was applied to the test data. Data was inverse transformed prior to plotting and metric calculations. Training data was split into 100 mini-batches per epoch.

The generator and critic loss functions were as proposed in Gulrajani et al. (2017) with gradient penalty added to the critic loss. Training was performed with an Adam optimizer with momentum parameters (β s) set to 0.5 and 0.9. The coefficient of gradient penalty was set at 0.1. We note that when using the same generator and critic architectures, but with other data (Hossain et al., 2021), we have found robust behavior of the predictions over a wide range of values for the coefficient of gradient penalty (0.01 to 10). A learning rate of $1e-3$ was used. The generator was only updated every 5th step in order to allow the critic to learn the Wasserstein distance function better before updating the generator.

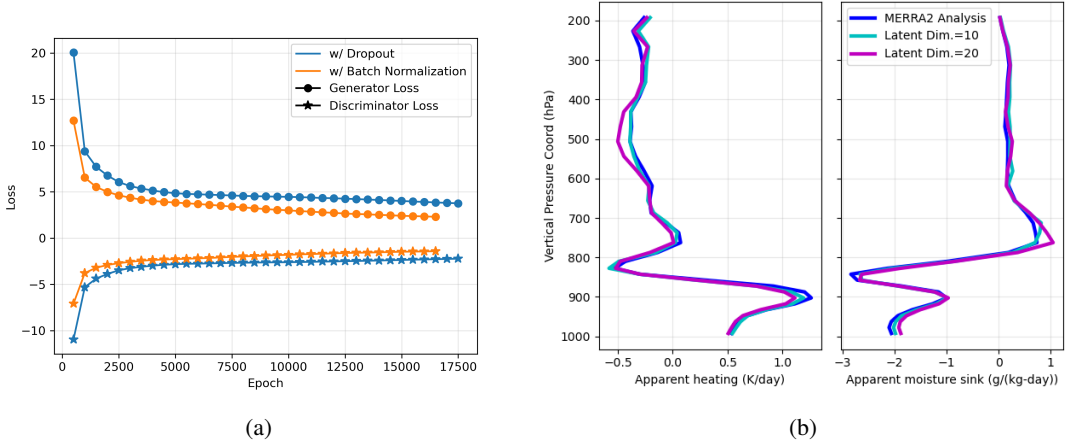


Figure 2. (a): Training loss with dropout (blue) and with batch normalization as a function of training epoch. Both generator and discriminator losses are shown and the training is seen to continue stably over large numbers of epochs. (b): Comparison of vertical distribution of cGAN predictions against reference MERRA2 analysis. Averages over test set of apparent heating (left) and apparent moisture sink (right) are compared. Teal (Magenta) values are for the case when the dimension of the noise vector is ten (twenty).

Once training was complete, the test conditions along with noise samples were fed to the generator to produce results that we discuss in the next section.

Variations of hyperparameter considered consisted of number of neurons in each layer, number of layers, activation function, coefficient of gradient penalty in discriminator loss, dropout and batch normalization layers in generator, and the dimension of the noise vector input to the generator. No sensitive dependencies were found. Furthermore, a validation set was not used for the reason that the training of the cGAN was stable and no special stopping criterion was used. For example, the averaged generator and discriminator loss functions were monotonic and could be continued for tens of thousands of epochs (see Fig. 2a for an example).

4. Results

Given the physics of the problem, and as described earlier, we focus on the vertical distributions of apparent heating and moisture sink, conditioned on the vertical distributions of temperature and specific humidity. Figure 2b shows comparisons of the vertical distribution of cGAN predictions against reference MERRA2 analysis. Here, averages over the test set are compared, with apparent heating shown in the left panel and the apparent moisture sink shown in the right panel. Two sets of cGAN predictions are shown with the only change being the dimension of the noise vector (cyan: 10, magenta: 20). The overall structure of the vertical distribution of both heating and moisture sink are reasonably well captured by the cGAN predictions with no indication of bias.

In more detail, in Fig. 3a, we consider the probability distributions over the test set at each pressure level with red indicating high probability and blue indicating low probability. Apparent heating is shown in the left column and apparent moisture sink in the right column. Reference MERRA2 analysis is shown in the top row and cGAN predictions (noise vector dimension ten) in the bottom row. The pdfs of the cGAN predictions are seen to compare well with the reference MERRA2 analysis. In particular, the predictions capture the skewed nature of the distributions well. However, the regions of high probability (width of red regions) in the pdfs of the cGAN predictions of heating, are seen to be slightly sharper

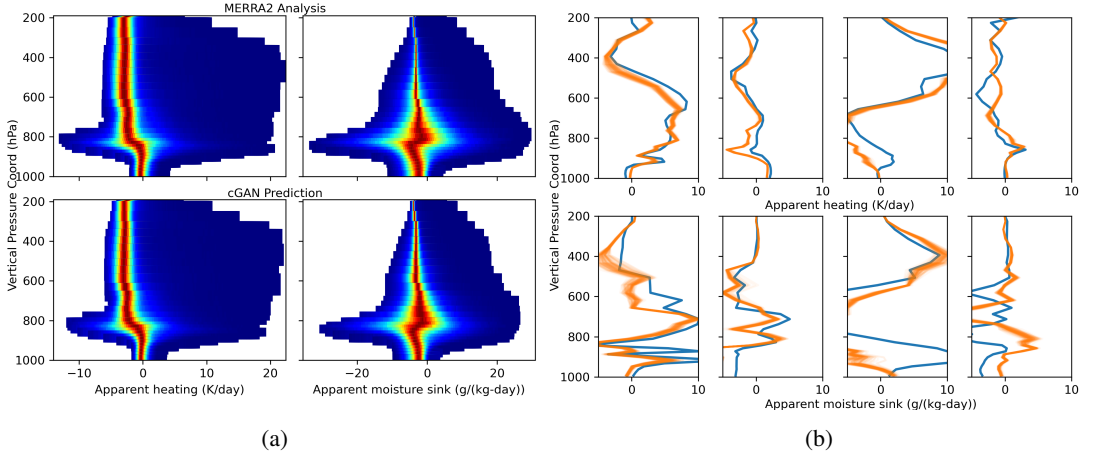


Figure 3. (a): The probability distribution functions (pdf; red: high probability; blue: low probability) over the test set are computed at each pressure level and compared against the MERRA2 pdfs. The variable depth of the MERRA2 vertical layers is apparent in these figures. Apparent heating is shown in the left column and apparent moisture sink is shown in the right column. Reference MERRA2 analysis is shown in the top row and cGAN predictions (noise vector dimension of ten) are shown in the bottom row. (b): A stochastic ensemble of cGAN predictions are shown for four random instances in the test set. The top row is for heating whereas the bottom row is for moisture sink. The reference MERRA2 profiles are shown in blue and the predictions in orange..

than in MERRA2 analysis. (With batch normalization, while the width of the mode region is as in MERRA2, a different minor discrepancy is seen: there are sharper jumps in the vertical.) For reference, at a yet more detailed level, we show stochastic ensembles of predictions at four randomly chosen test conditions in Fig. 3b. The reference MERRA2 profiles are shown in blue and the predictions in orange. Note that while the cGAN predictions sometimes appear as a thick orange line, they are actually an ensemble of thin lines. The stochastic ensemble was obtained by holding the test condition fixed while repeatedly sampling the noise vector. More often, the cGAN predictions are seen to better capture the slower variations.

5. Conclusion

The tropical Eastern Pacific is an important region for global climate and contains regions of intense tropical convection—segments of the ITCZ. Adopting a framework of apparent heating and apparent moisture sink to approximately separate the effects of dynamics and column-physics, we diagnosed the “physics” sources using the MERRA2 reanalysis product in a preprocessing step. We performed the analysis at MERRA2’s native spatiotemporal resolution, and then at a significantly coarser resolution. In both cases, we found that the heating and moisture sink were highly correlated with vertical advection of temperature and humidity (~ 0.9 , and -0.7) respectively.

Thereafter, we designed a probabilistic machine learning technique to learn the distribution of the heating and moisture sink profiles conditioned on vertical profiles of temperature and specific humidity. This was based on a Wasserstein Generative Adversarial Network with gradient penalty (WGAN-GP). After successfully training the cGAN, we were able to demonstrate the viability of the methodology to learn unified stochastic parameterizations of column physics by comparing predictions using test conditions against reference MERRA2 analysis profiles. We expect this work to add to the growing body of literature (e.g., Krasnopolsky et al., 2010, 2013; Rasp et al., 2018; O’Gorman

and Dwyer, 2018; Brenowitz and Bretherton, 2018, and others) that seeks to develop machine-learned column-physics parameterizations towards alleviating both, shortcomings of human-designed physics parameterizations, and the computational demand of the “physics” step in climate models.

We conclude by mentioning a few issues that need further investigation. Given the diversity of behavior (e.g., ITCZ vs. non-ITCZ regions), it remains to be seen if adding velocity fields as predictors will improve performance. Training over ITCZ regions and testing elsewhere and other such combinations are likely to render further insight into the parameterizations. The stochastic ensemble our method produces, e.g., like in Fig. 3b, can be readily subject to reliability and other analyses using tools developed in the context of probabilistic weather forecasts (e.g., see Nadiga et al., 2013; Luo et al., 2022, and references therein). We anticipate that such analyses will help us better understand the role played by the dimension of the latent space used in generative modeling. Finally, stability of the machine learned parameterization in a GCM setting is an important issue. For example, Brenowitz and Bretherton (2018) find this to be a problem when they learn *deterministic* parameterizations from CRM-based data. They circumvent the problem by changing the problem formulation to include time integration of the temperature (in their case static stability) and moisture equations and changing the loss function to penalize deviations of the predictions of T and q at multiple times in a cumulative sense. It remains to be seen if the *stochastic* parameterizations learned using a probabilistic ML methodology, as we do presently, can provide an alternative way of addressing the stability issue.

Funding Statement. This research was supported under U.S. Department of Energy (DOE), Office of Science’s Scientific Discovery through Advanced Computation (SciDAC4) program under project “Non-Hydrostatic Dynamics with Multi-Moment Characteristic Discontinuous Galerkin Methods (NH-MMCDG)”.

Competing Interests. None

Data Availability Statement. MERRA2 data used in this work is available and can be downloaded at <https://disc.gsfc.nasa.gov/datasets?project=MERRA-2>

Author Contributions. Conceptualization: BTN, Methodology: BTN, CN. Data curation: BTN, XS. Data visualisation: BTN Writing original draft: BTN. All authors approved the final submitted draft.

References

- Arjovsky, M. and Bottou, L. (2017). Towards principled methods for training generative adversarial networks. *arXiv preprint arXiv:1701.04862*.
- Bosler, P. A., Bradley, A. M., and Taylor, M. A. (2019). Conservative multimoment transport along characteristics for discontinuous galerkin methods. *SIAM Journal on Scientific Computing*, 41(4):B870–B902.
- Bradley, A. M., Bosler, P. A., Guba, O., Taylor, M. A., and Barnett, G. A. (2019). Communication-efficient property preservation in tracer transport. *SIAM Journal on Scientific Computing*, 41(3):C161–C193.
- Brenowitz, N. D. and Bretherton, C. S. (2018). Prognostic validation of a neural network unified physics parameterization. *Geophysical Research Letters*, 45(12):6289–6298.
- Chen, D., Rojas, M., Samset, B., Cobb, K., Niang, A. D., Edwards, P., Emori, S., Faria, S., Hawkins, E., Hope, P., et al. (2021). Framing, context, and methods. *Climate Change*.
- Coifman, R. R. and Lafon, S. (2006). Diffusion maps. *Applied and computational harmonic analysis*, 21(1):5–30.
- Duan, J. and Nadiga, B. (2007). Stochastic parameterization for large eddy simulation of geophysical flows. *Proceedings of the American Mathematical Society*, 135(4):1187–1196.
- Goodfellow, I., Pouget-Abadie, J., Mirza, M., Xu, B., Warde-Farley, D., Ozair, S., Courville, A., and Bengio, Y. (2014). Generative adversarial nets. *Advances in neural information processing systems*, 27.
- Gulrajani, I., Ahmed, F., Arjovsky, M., Dumoulin, V., and Courville, A. (2017). Improved training of wasserstein gans. *arXiv preprint arXiv:1704.00028*.
- Herman, G. R. and Schumacher, R. S. (2016). Extreme precipitation in models: An evaluation. *Weather and Forecasting*, 31(6):1853–1879.
- Hossain, M., Nadiga, B. T., Korobkin, O., Klasky, M. L., Schei, J. L., Burby, J. W., McCann, M. T., Wilcox, T., De, S., and Bouman, C. A. (2021). High-precision inversion of dynamic radiography using hydrodynamic features. *arXiv preprint arXiv:2112.01627*.
- Kantorovitch, L. (1958). On the translocation of masses. *Management science*, 5(1):1–4.
- Kingma, D. P. and Welling, M. (2013). Auto-Encoding Variational Bayes. *arXiv e-prints*, page arXiv:1312.6114.

- Krasnopolsky, V., Fox-Rabinovitz, M., Hou, Y., Lord, S., and Belochitski, A. (2010). Accurate and fast neural network emulations of model radiation for the NCEP coupled climate forecast system: climate simulations and seasonal predictions. *Monthly Weather Review*, 138(5):1822–1842.
- Krasnopolsky, V. M., Fox-Rabinovitz, M. S., and Belochitski, A. A. (2013). Using ensemble of neural networks to learn stochastic convection parameterizations for climate and numerical weather prediction models from data simulated by a cloud resolving model. *Advances in Artificial Neural Systems*, 2013.
- Lean, H. W., Clark, P. A., Dixon, M., Roberts, N. M., Fitch, A., Forbes, R., and Halliwell, C. (2008). Characteristics of high-resolution versions of the met office unified model for forecasting convection over the united kingdom. *Monthly Weather Review*, 136(9):3408–3424.
- Luo, X., Nadiga, B. T., Ren, Y., Park, J. H., Xu, W., and Yoo, S. (2022). A bayesian deep learning approach to near-term climate prediction. *Journal of Advances in Modeling Earth Systems*, 14.
- Nadiga, B. (2008). Orientation of eddy fluxes in geostrophic turbulence. *Philosophical Transactions of the Royal Society A: Mathematical, Physical and Engineering Sciences*, 366(1875):2489–2508.
- Nadiga, B. and Livescu, D. (2007). Instability of the perfect subgrid model in implicit-filtering large eddy simulation of geostrophic turbulence. *Physical Review E*, 75(4):046303.
- Nadiga, B. T., Casper, W. R., and Jones, P. W. (2013). Ensemble-based global ocean data assimilation. *Ocean Modelling*, 72:210–230.
- Nitta, T. (1977). Response of cumulus updraft and downdraft to gate a/b-scale motion systems. *Journal of Atmospheric Sciences*, 34(8):1163–1186.
- O’Gorman, P. A. and Dwyer, J. G. (2018). Using machine learning to parameterize moist convection: Potential for modeling of climate, climate change, and extreme events. *Journal of Advances in Modeling Earth Systems*, 10(10):2548–2563.
- Palmer, T. (2019). Stochastic weather and climate models. *Nature Reviews Physics*, 1(7):463–471.
- Rasp, S., Pritchard, M. S., and Gentine, P. (2018). Deep learning to represent subgrid processes in climate models. *Proceedings of the National Academy of Sciences*, 115(39):9684–9689.
- Rezende, D. and Mohamed, S. (2015). Variational inference with normalizing flows. In *International conference on machine learning*, pages 1530–1538. PMLR.
- Rienecker, M. M., Suarez, M. J., Gelaro, R., Todling, R., Bacmeister, J., Liu, E., Bosilovich, M. G., Schubert, S. D., Takacs, L., Kim, G.-K., et al. (2011). Merra: Nasa’s modern-era retrospective analysis for research and applications. *Journal of climate*, 24(14):3624–3648.
- Sherwood, S. C., Bony, S., and Dufresne, J.-L. (2014). Spread in model climate sensitivity traced to atmospheric convective mixing. *Nature*, 505(7481):37–42.
- Sun, X. and Barros, A. P. (2014). High resolution simulation of tropical storm ivan (2004) in the southern appalachians: role of planetary boundary-layer schemes and cumulus parametrization. *Quarterly Journal of the Royal Meteorological Society*, 140(683):1847–1865.
- Sun, X. and Barros, A. P. (2015). Isolating the role of surface evapotranspiration on moist convection along the eastern flanks of the tropical andes using a quasi-idealized approach. *Journal of Atmospheric Sciences*, 72(1):243–261.
- Weisman, M. L., Davis, C., Wang, W., Manning, K. W., and Klemp, J. B. (2008). Experiences with 0–36-h explicit convective forecasts with the wrf-arw model. *Weather and Forecasting*, 23(3):407–437.
- Yanai, M., Esbensen, S., and Chu, J.-H. (1973). Determination of bulk properties of tropical cloud clusters from large-scale heat and moisture budgets. *Journal of Atmospheric Sciences*, 30(4):611–627.
- Zhang, G., Cook, K. H., and Vizi, E. K. (2016). The diurnal cycle of warm season rainfall over west africa. part ii: Convection-permitting simulations. *Journal of Climate*, 29(23):8439–8454.